

Chronic stress-induced disruption of the astrocyte network is driven by structural atrophy and not loss of astrocytes

Ross J. Tynan · Sarah B. Beynon · Madeleine Hinwood ·
Sarah J. Johnson · Michael Nilsson ·
Jason J. Woods · Frederick R. Walker

Received: 28 September 2012/Revised: 24 January 2013/Accepted: 12 February 2013/Published online: 20 March 2013
© Springer-Verlag Berlin Heidelberg 2013

Abstract Chronic stress is well recognized to decrease the number of GFAP⁺ astrocytes within the prefrontal cortex (PFC). Recent research, however, has suggested that our understanding of how stress alters astrocytes may be incomplete. Specifically, chronic stress has been shown to induce a unique form of microglial remodelling, but it is not yet clear whether astrocytes also undergo similar structural modifications. Such alterations may be significant given the role of astrocytes in modulating synaptic function. Accordingly, in the current study we have examined changes in astrocyte morphology following exposure to chronic stress in adult rats, using three-dimensional digital reconstructions of astrocytes. Our analysis indicated that chronic stress produced profound atrophy of astrocyte process length, branching and volume. We additionally examined changes in astrocyte-specific S100 β , which are both a putative astrocyte marker and a protein whose expression is associated with

astrocyte distress. While we found that S100 β levels were increased by stress, this increase was not correlated with atrophy. We further established that while chronic stress was associated with a decrease in astrocyte numbers when GFAP labelling was used as a marker, we could find no evidence of a decrease in the total number of cells, based on Nissl staining, or in the number of S100 β ⁺ cells. This finding suggests that chronic stress may not actually reduce astrocyte numbers and may instead selectively decrease GFAP expression. The results of the current study are significant as they indicate stress-induced astrocyte-mediated disturbances may not be due to a loss of cells but rather due to significant remodeling of the astrocyte network.

Keywords Astrocyte · Chronic stress · GFAP · S100 β · Infralimbic prefrontal cortex

R. J. Tynan · S. B. Beynon · M. Hinwood ·
J. J. Woods · F. R. Walker (✉)
School of Biomedical Sciences and Pharmacy, The University
of Newcastle, University Drive, Callaghan, Newcastle,
NSW 2308, Australia
e-mail: rohan.walker@newcastle.edu.au

R. J. Tynan · S. B. Beynon · M. Hinwood · M. Nilsson ·
J. J. Woods · F. R. Walker
Centre for Brain and Mental Health Research,
University of Newcastle, Newcastle, NSW, Australia

S. J. Johnson
School of Electrical Engineering and Computer Science,
The University of Newcastle, University Drive, Callaghan,
Newcastle, NSW 2308, Australia

R. J. Tynan · S. B. Beynon · M. Hinwood · M. Nilsson ·
J. J. Woods · F. R. Walker
Hunter Medical Research Institute, Newcastle, NSW, Australia

Introduction

Exposure to chronically stressful situations is recognized to be one of the most significant risk factors in the emergence of clinically diagnosable depression [25]. While the neuronal disturbances induced by exposure to chronic stress have been extensively characterized, particularly within susceptible forebrain regions such as the medial prefrontal cortex (PFC, [42, 43]), considerably less is known about the effect of stress on glia.

Using an animal model of chronic stress, our research group has recently demonstrated that in addition to eliciting a substantial increase in anhedonic-like behaviour [57] and producing a deficit in working memory [26], chronic stress led to pronounced remodelling of microglia within the ventromedial PFC [27]. Specifically, the results from these studies revealed that chronic stress significantly increased

the internal complexity of microglia, by enhancing ramification (cellular branching) without altering the overall area occupied by the cell. These findings not only suggest the involvement of microglial ramification in mediating stress-induced behavioural effects, but also clearly demonstrate the potential of chronic stress to significantly modify glial morphology within the PFC.

Like microglia, astrocytes are also responsive to the effects of chronic stress. In one of the first studies to directly examine this relationship, Czeh et al. [13] revealed that tree shrews exposed to 5 weeks of chronic psychosocial stress exhibited significantly reduced numbers of glial fibrillary acidic protein (GFAP) positive astrocytes in the hippocampus. This study was important not only because the work was done in a close analogue of primates, but also because of the use of unbiased stereological assessments (based on the optical fractionator method), which currently represents the highest standard of evidence for determining changes in cellular density. In a seminal investigation that followed, Banasr and Duman [4] significantly expanded upon these findings, by firstly demonstrating that chronic unpredictable mild stress could induce a reduction in astrocyte (GFAP⁺) density within the rat PFC; and secondly, by highlighting the crucial role of astrocytes in mediating behaviour, by showing that specific pharmacological ablation of astrocytes induced depressive-like behaviour similar to that observed following exposure to chronic stress. The translational significance of these results is considerable, as they are consistent with findings demonstrating that the number of glia within the PFC of post-mortem tissue taken from individuals with a life history of depression is significantly reduced (succinctly reviewed by [45–47]). Together, these studies suggest that a reduced number of GFAP⁺ astrocytes within the PFC may drive the emergence of stress-linked behavioural changes and could under certain circumstances contribute to the emergence of mood disturbances.

One potentially important caveat to the proposed link between astrocyte cell loss and the emergence of cognitive disturbance is the reliance on GFAP as an immutable marker for astrocytes. There have now been several studies that have shown that certain conditions can dramatically increase GFAP [49, 60] or produce a specific decrease in GFAP without any appreciable change in cell number [22]. In these situations, density assessments based on GFAP would indicate that a change in cell number has occurred, when in fact all that may have changed are the expression of the protein upon which density estimates were based. Whether the reported decrease in astrocyte numbers following stress represents a *bona fide* reduction in cell number has yet to be directly confirmed.

The protein S100 β is widely recognized to be associated with astrocyte distress, and is particularly concentrated in astrocytes within the central nervous system (CNS). Due to this property, S100 β has been extensively used as a surrogate marker of astrocytes [32, 50]. However, S100 β has also been

identified to possess a number of distinct functional roles. For instance, elevated circulating levels of S100 β have been commonly observed in a variety of neurodegenerative conditions such as multiple sclerosis [39] and Alzheimer's disease [58], and more recently in individuals with depression [2, 51]. Due to its detection in neurodegenerative disease, it was originally proposed that the elevations in S100 β were the consequence of damaged cells within the CNS (see [34] for review). It is now well recognized that S100 β can be actively released, exerting protective neurotrophic effects at low concentrations [29] and potentially harmful effects at higher concentrations, by increasing cyclooxygenase-2 expression and free radical release [8, 28, 29]. To date, the expression of S100 β in response to chronic stress has not been characterized.

While changes in astrocyte density are obviously important, there is reason to believe that chronic stress may also drive significant structural remodelling of astrocytes. Astrocytes are exquisitely sensitive to changes in their extracellular environment [1], and like microglia, their structure is intimately linked with their function [33, 35]. Such remodelling may be significant given that each astrocyte is known to be capable of making contact with, and modulating the activity of, many thousands of individual synapses [10]. However, no studies to our knowledge have yet examined whether astrocyte morphology can be disturbed by exposure to chronic stress.

The primary aim of the current study was to assess how astrocyte morphology is altered by exposure to chronic stress. We have addressed this issue by creating high-resolution three-dimensional reconstructions of astrocytes, from each of the distinct anatomical layers within the PFC, and quantitatively examined changes in their structure. We have chosen to examine changes in astrocytes across layers, as it is well recognized that there are distinct afferent and efferent inputs into each layer [14], and such a laminar analysis will give insight into which functions and brain regions are likely to be most influenced (if at all). We have assessed changes in GFAP density using stereology, exhaustive counting and thresholding-based assessments and have undertaken an independent assessment of cell density using Nissl-based stereological counting and counts of S100 β ⁺ cells. Finally, given findings indicating that circulating S100 β is elevated in depression, and its dose-dependent Jekyll and Hyde properties within the CNS, we examined the relationship between S100 β and astrocyte remodelling and density within the PFC.

Materials and methods

Animals

All experiments used adult male Sprague–Dawley rats (70-day old at the commencement of the experiment;

~350–450 g) obtained from the Animal Resource Centre (Perth, Western Australia). Animals were maintained in a temperature (21 ± 1 °C) and humidity controlled environment, with food and water available ad libitum. Lighting was on a 12:12-h reverse light–dark cycle (lights on 1900 hours), with all experimental procedures conducted in the dark phase under low level red lighting (40 Lux). Prior to the commencement of experimentation, all animals were individually housed and given a minimum of 7 days acclimation. All procedures were approved by the University of Newcastle Animal Care and Ethics Committee, and conducted in accordance with the New South Wales Animals Research Act and the Australian Code of Practice for the use of animals for scientific purposes.

Experimental procedure

Animals were randomly allocated into either a chronic stress ($n = 10$) or handled control ($n = 10$) condition, with both treatments consisting of a 21-day experimental protocol. The chronic stress procedure involved restraining animals as described previously [26, 27]. This model was chosen because it produces robust decreases in dendritic length and spine density, particularly within the PFC, that does not occur when shorter exposure periods are utilized [1, 4, 32, 43].

In brief, animals were placed within wire mesh (0.6 mm diameter, 6.5×6.5 mm grid) restrainers secured with butterfly clips for 6 h each day of the 21-day protocol. The handling procedure for control animals was designed to emulate the stress protocol, minus the restraint. Thus, each animal was individually removed from their home cage, held for approximately 2 min, and then returned to their home cage, twice each day throughout the 21-day protocol. Furthermore, for the duration of the 6-h stress period, animals in the handled control condition had their food and water access removed.

Tissue preparation

All animals were deeply anaesthetized (sodium pentobarbital, 80 mg/kg i.p.) and transcardially perfused via the ascending aorta 24 h after cessation of the final stress episode. Tissue was cleared with 300 ml of 0.1 M phosphate buffer (PB) solution containing 2 % sodium nitrite (pH 7.40), and then subsequently fixed using 400 ml of 4 % paraformaldehyde in 0.1 M PB. Brains were extracted and placed in the same fixative solution for 16 h, and then blocked at the base of the midbrain before being placed in a 12.5 % sucrose solution in 0.1 M PB (pH 7.40, 4 °C) overnight for cryoprotection. Serial coronal sections were sliced using a freezing (-25 °C) microtome (Leica SM 2000R) at 30- μ m intervals. Sections were divided into a

1-in-6 series and stored in anti-freeze solution (4 °C) until required for immunoperoxidase or immunofluorescent labelling.

Immunoperoxidase labelling

For all immunohistochemistry, sections from both stress and control groups were processed simultaneously to avoid any possible artefacts as a consequence of the labelling procedure. Sections were rinsed with 0.1 M PB before the endogenous peroxidases were destroyed in 0.1 M PB containing 1 % H_2O_2 , with non-specific binding then blocked by incubation in 0.1 M PB solution containing 3 % normal horse serum. Sections were then incubated with a rabbit polyclonal antiserum directed against GFAP (1:5,000; Millipore) or S100 β (1:4,000; Sigma-Aldrich) in phosphate buffered horse serum (PBH) for 72 h at 4 °C. Sections were then washed in 0.1 M PB, incubated with a biotinylated donkey anti-mouse or -rabbit secondary antibody (1:300, Jackson Immunoresearch) in PBH for 2 h, rinsed, and then incubated in 0.1 % extravidin peroxidase (1:1,000; Sigma-Aldrich) for 1 h before being rinsed again. The immunolabelling was then developed using a nickel-enhanced 3,3'-diaminobenzidine solution, which was closely monitored under a microscope until optimal staining with minimal background labelling was achieved (5 min). Sections were then mounted onto chrome alum-coated slides, dehydrated using a graded series of ethanol (70 %, 95 %, 100 %, absolute), cleared in xylene and coverslipped.

Immunofluorescent labelling

As for immunoperoxidase, all immunofluorescently labelled sections were processed simultaneously to avoid any possible non-specific differences as a consequence of the labelling procedure. Initially, sections were rinsed three times in 0.1 M phosphate buffered saline (PBS; pH 7.40), followed by a 1-h incubation in 0.1 M PBS containing 3 % bovine serum albumin (BSA) and 0.3 % Triton X-100. Sections were then transferred into a 1 % BSA and 0.1 % Triton X-100 solution containing appropriate primary antibodies (anti-mouse GFAP, 1:200, Millipore; anti-mouse S100 β , 1:4,000, Sigma-Aldrich; or anti-rabbit GFAP, 1:100, Millipore) and incubated overnight at 4 °C. Sections were next rinsed three times in 0.1 M PBS, and then incubated in a 1 % BSA and 0.1 % Triton X-100 solution containing appropriate fluorescent secondary antibodies (anti-mouse AlexaFluor-488 or anti-rabbit AlexaFluor-594, 1:400, Invitrogen). To determine the extent of co-localization, sections were double labelled using a sequential labelling process. After processing was complete, sections were rinsed, mounted onto chrome alum-coated slides, and coverslipped.

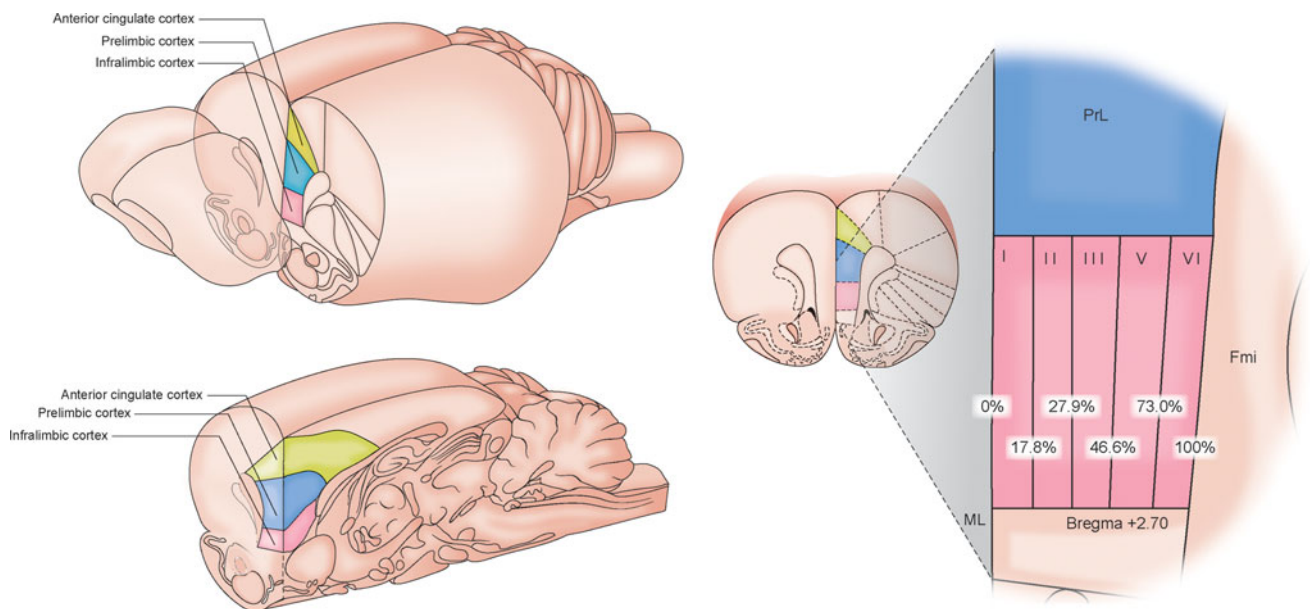


Fig. 1 The anatomical locus of the medial prefrontal cortex within the rat brain. The *left panel of images* shows the prefrontal cortex from both coronal (*upper*) and sagittal (*lower*) views, respectively. The *image on the right* shows a coronal section, with the *inset image*

illustrating the relative cortical depths of each layer within the IL cortex (*ML* midline, *PrL* prelimbic cortex, *Fmi* forceps minor). Adapted from Paxinos and Watson [38]

Analysis of the infralimbic cortex

All analysis was conducted by an independent trained observer, blind to experimental conditions. To prevent identification of the experimental treatments, all tissues were assigned a random numerical coding, which was not broken until all processing were complete. For both immunoperoxidase and immunofluorescent labelled tissues, all sections were obtained from rostrocaudal levels within the range of approximately +2.20 and +3.20 mm from Bregma, according to the Paxinos and Watson rat brain atlas [38]. For initial observations, changes in GFAP immunoreactivity were investigated with regard to the total infralimbic (IL) cortex. Subsequent analysis involved separating this region into layers, which was achieved by firstly assigning the distance from the pial surface to the underlying white matter of the forceps minor a value of 100 %. This value was then divided into cortical layer depths previously established for the Sprague–Dawley rat [19], and used in many recent publications [26, 36], with the width of each layer defined as I (17.8 %), II (27.9 %), III (46.6 %), V (73.0 %) and VI (100 %), as shown in Fig. 1.

Acquisition of images for three-dimensional reconstructions of astrocytes

Digital reconstructions of astrocytes were based on confocal images of GFAP-labelled tissue acquired using a computer-

assisted morphometry system. This consisted of a Nikon Eclipse 80i confocal microscope equipped with a motorized z-stage, which was connected to a Dell PC running EZ-C1 confocal microscope software (Gold Version 3.80; Nikon Corporation). Confocal Stacks (50–100 images separated by a 0.25- μm z-axis step size) of GFAP-immunolabelled tissue were acquired using a Nikon Plan VC 100 \times objective (oil immersion, N.A. 1.4; see Fig. 2a, b). Each image was taken at a resolution of 1,024 \times 1,024 pixels, with the pixel dwell time set to 3.36 μs , giving a rate of 0.185 z-planes per second. Additional settings including gain, offset and pin-hole size were optimized prior to imaging, with these settings held constant for all subsequent analysis. To be included for reconstruction, cells needed to fulfil each of the following criteria: (1) the cell must be located within layers II, III, V or VI of the IL cortex; (2) the entire cell must reside completely within the z depth of the section; and (3) each cell must have intact astrocyte processes unobscured by neighbouring cells or background immunolabelling. Layer I of the IL PFC was excluded from analysis due to the high density of GFAP⁺ cells within the layer preventing reliable reconstruction of single cells (see Fig. 2d). Astrocytes were also excluded from analysis if they were surrounding blood vessels or capillaries. From each animal three cells were pseudo-randomly selected for reconstruction from within the IL PFC, with one cell representing the top, middle and bottom of each of the four measured IL PFC layers. This produced a total of 240 reconstructed cells (120 stress, 120 controls) comprised 60 cells from each layer (30

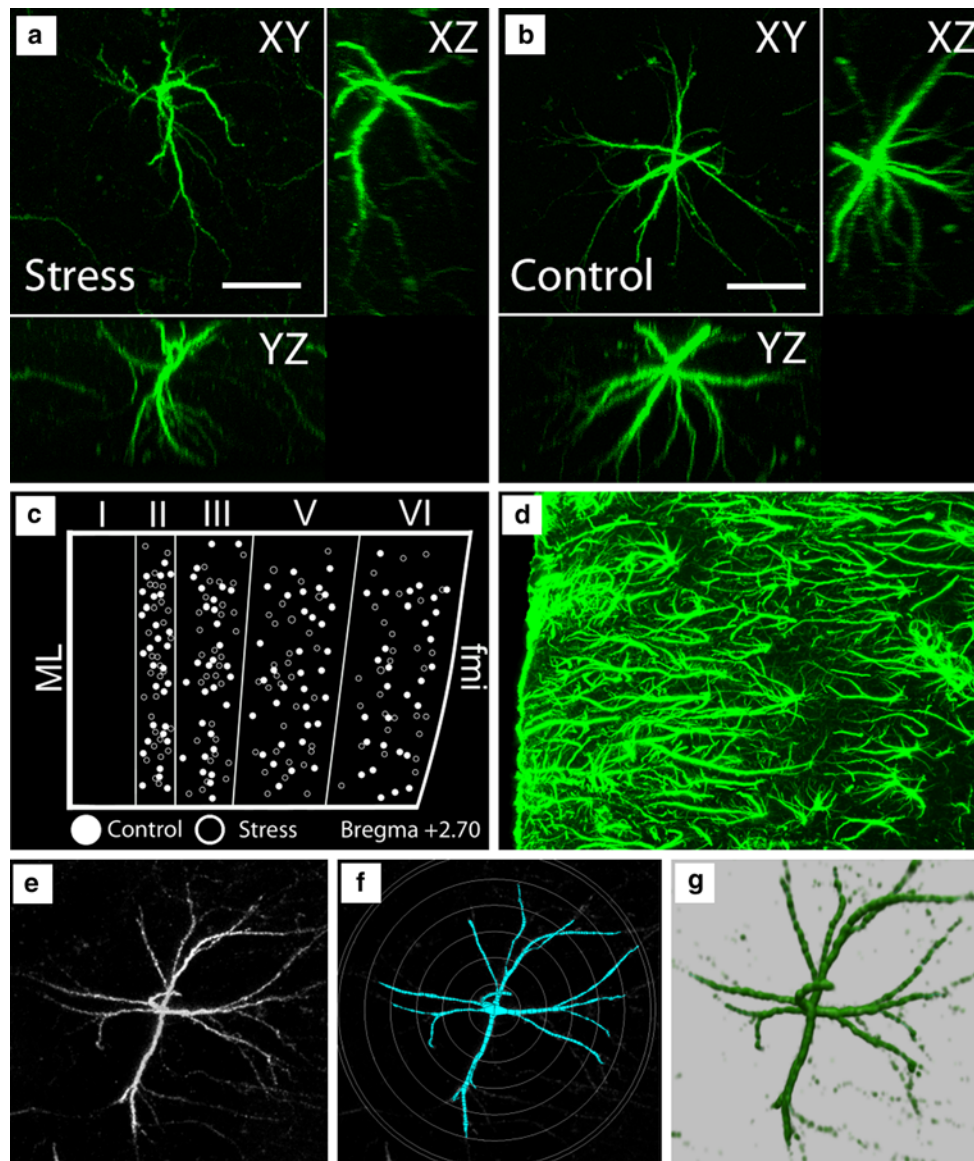


Fig. 2 Illustration of the 3D reconstruction process. Maximum intensity projections of confocal stacks were acquired for reconstruction of both stress (**a**) and control (**b**) cells, with views from the corresponding *XY* and *XZ* planes (scale bar 20 μ m). The anatomical locations of the scan sites within each of the cortical layers of the IL cortex that were sampled for reconstruction in both stress and control

stress, 30 controls). Figure 2c shows the distribution of scan sites recorded within the IL PFC.

Image processing of acquired images and digital reconstruction

Prior to reconstruction, all raw images collected were attenuation corrected using AutoDeblur (Version X2; AutoQuant X, Media Cybernetics Inc.), to minimize any loss in colour intensity as a consequence of photobleaching. This process was then followed by a 3D blind

tissue are shown (c). A significant degree of overlap in cells within layer I of the IL cortex prevented reliable reconstruction of individual cells (d). The final three images illustrate the reconstruction process, with raw tissue (e); the detection of the cell in Neuronstudio software, with the surrounding Sholl rings (f); and the final 3D reconstruction (g)

deconvolution (10 iterations) to compensate for optical aberrations and enhance contrast and resolution, producing a greyscale image that was saved in a tiff format. Finally, all images were processed in NeuronStudio, a software package that digitizes deconvolved confocal laser scanning microscopy stacks and creates a 3D reconstruction suitable for morphometric analysis. The software initially detects the medial axis of the cell by connecting chains of voxels. The diameter is then determined using a Rayburst sampling algorithm, where rays are sent from the centre of a lighted structure (medial axis), until they reach a given exit

condition where they stop, allowing accurate measurement of non-symmetrical 3D process shapes and providing precise detection of process length and volume [59]. This software is freely available to download from the Computational Neurobiology and Imaging Centre webpage <http://research.mssm.edu/cnic/tools-ns.html>. After reconstruction, summary statistics were generated using a 3D Sholl analysis with concentric spheres surrounding the origin of the cell, with the initial sphere 3 μm in diameter, with each subsequent sphere increasing in 3- μm radial increments. The 3D Sholl analysis provided quantification of the following parameters: process length, process volume and the number of branch points for the total cell, and proportionately across each of the Sholl spheres. Figure 2 (e, f, g) briefly illustrates the reconstruction process.

Density estimates of GFAP⁺ immunoreactive material

To further investigate stress-induced changes, the immunofluorescently labelled tissue was processed to determine the total density of GFAP⁺ immunoreactive material within the IL PFC. A low magnification (10 \times , N.A. 0.45) confocal stack (1,024 \times 1,024 resolution, step size 5 μm) of images was acquired using a Nikon Eclipse 80i confocal microscope with EZ-C1 software (Gold Version 3.80). A maximum intensity projection of the image stack was then produced using NeuroLucida (Version 10.30.1, 64 bit; MBF Biosciences), with the percentage of immunoreactive material then quantified as described previously [57]. In brief, this involved a thresholding procedure using Metamorph software (version 7.5.4.0; Molecular Devices), whereby only pixels within a predetermined range of colour intensity were included for analysis. The colour threshold was set so that all cell bodies and associated processes were thresholded, with the density of immunoreactive material then determined by quantifying the percentage of thresholded material within the region of interest (ROI), in this case being the IL PFC. Subsequently, the same thresholding procedure was used to investigate the density of GFAP within each layer of the IL PFC. Five ROIs were made (one for each layer) within the IL PFC corresponding to the predetermined size of each layer. Finally, a separate set of cells from the primary motor cortex, a region not known to display astrocyte changes in response to stress, were also processed for comparison to those in the IL PFC.

Stereological estimates of GFAP⁺ astrocytes and total cell numbers within the IL PFC

The number of GFAP⁺ astrocytes within the IL PFC was quantified by systematically sampling the tissue using StereoInvestigator software (version 8.27, MBF

Bioscience, Williston, Vermont). Live video images of immunoperoxidase-labelled GFAP⁺ cells were viewed using a Zeiss Axioskop photomicroscope equipped with a MAC 6000 XYZ computer-controlled motorized stage with joystick and focus control (Ludl Electronic Products), a Q Imaging video camera (MBF Biosciences), and a PC running Windows 7 (Dell Australia). Initially, the perimeter of the IL PFC was traced at a low magnification (4 \times , N.A. 0.1), with the boundaries of the individual layers demarcated at sizes previously defined [Layer I (17.8 %), II (27.9 %), III (46.6 %), V (73.0 %) and VI (100 %)]. Cells were then counted over three separate sections (inter-section interval of 6) at a high magnification (40 \times , N.A. 0.65). Counting frames (90 \times 90 μm) were systematically sampled within a grid with constant dimensions (125 \times 125 μm), yielding approximately 300–320 sampling sites per animal. Due to shrinkage of the tissue after immunohistochemical processing and coverslipping procedures, the average measured tissue thickness was $22.6 \pm 0.5 \mu\text{m}$. As such, we used an optical dissector of 20 μm with a 1- μm guard zone for all counting. GFAP⁺ astrocyte cells were counted only if their cell body came into focus within the height of the dissector probe, and were clearly within the perimeter of the counting frame without intersecting the exclusion lines. A similar procedure was used to investigate the total cell population, with stereological estimates of the number of cells in a series of six Nissl-stained tissue sections (inter-section interval of 6). On average, 20 sites were sampled for each section across a grid of 175 \times 200 μm , with randomly placed counting frames of 50 \times 50 μm . Cells were only included in the analysis if the nucleus came into focus within the height of the optical dissector (7 μm with a 5- μm guard zone).

Exhaustive counting of GFAP⁺ cells within the IL PFC

Using the same tissue sections and microscope as used for counting with the optical fractionator, we investigated the distribution of astrocyte cells within the IL PFC. A low magnification image of the IL PFC (10 \times , N.A. 0.25) was captured and then imported into Photoshop CS6 (version 13.0 \times 64, Adobe Systems Inc.). A transparent layer was added above each image, onto which 2-mm dots were digitally placed directly above each GFAP-positive cell. This process created a dot plot similar to that created using the optical fractionator method. This approach, however, allowed us to determine the precise XY location of each GFAP positive cell. Specifically, this was achieved by importing the dot plots into Metamorph software (version 7.5.4.0; Molecular Devices) where a ROI corresponding to the IL PFC was overlaid, and the co-ordinates of all cells within this region were recorded using integrated morphometry analysis. Cellular co-ordinates were then

extracted and processed in Matlab (version 7.9.0.529 [R2009b], The Mathworks, Inc). In brief, the IL PFC region was divided into a grid of 7×10 equally sized squares, and the number of cells in each square counted. These counts were then used to generate heat maps illustrating the distribution of cellular density.

Intrasomal and extrasomal intensity of S100 β and S100 β^+ cell counts

We next investigated the impact of chronic stress on both the intra- and extracellular expressions of S100 β . Confocal stacks (50–100 images separated by a 0.25- μm z step size; 100 \times magnification) of tissue co-labelled with S100 β and GFAP were acquired on a Nikon Eclipse microscope, which were then imported into NeuroLucida (version 10.30.1, 64bit; MBF Biosciences) to create a maximum intensity projection. The density of intrasomal S100 β was then quantified by tracing a perimeter surrounding S100 β positive cells, and recording the colour intensity using Metamorph (version 7.5.4.0; Molecular Devices). Extrasomal S100 β expression was measured using a similar colour intensity procedure, whereby four equally sized square ROIs were systematically placed in fixed positions within each corner of the image. We also undertook an exhaustive account of S100 β^+ cells using the method described above for GFAP $^+$ cells.

Data analysis

All data were analyzed using the Statistical Package for Social Sciences (SPSS, version 19; IBM). Evaluation of the threshold and intensity data from GFAP- and S100 β -immunolabelled tissue was conducted using an independent sample t test with ‘Stress group’ as the between subject variable (two levels: stress, control). For all analyses involving multiple layers within the IL PFC, we conducted multivariate ANOVAs, with ‘Stress group’ (two levels: stress, control) and ‘layer’ as between subject variables (five levels: I, II, III, V and VI). We used these same variables for the morphometric analysis of the 3D astrocyte reconstructions, with the addition of a further between-subject variable ‘Sholl ring’ (12 levels: 3, 6, 9, 12, 15, 18, 21, 24, 27, 30, 33 and 36). Planned comparisons between average morphometric values for each subject from stress ($n = 10$) and control ($n = 10$) groups were conducted. The relationship between S100 β and astrocyte morphological parameters (process length, volume and number of branches) and astrocyte density (optical fractionator estimates) were determined using Pearson’s correlation. For all analyses, planned comparisons of simple effects and Tukey’s post hoc tests were used to identify the location of any significant differences both between and within groups.

In all cases, ANOVA assumptions including the homogeneity of variance, homogeneity of regression and sphericity were satisfied. Data are expressed as mean values \pm SEM for all experimental groups, with the α criterion set at $p < 0.05$.

Results

Changes in the IL astrocyte process length

Within each layer, process length was assessed by calculating and comparing to the total length of all cellular processes, and then further investigated by comparing the process length within each of the concentric Sholl spheres. Irrespective of treatment condition or layer, Sholl analysis showed that on average greater than 90 % of all process length occurred within 18 μm of the cell origin. Animals exposed to chronic stress ($M = 148.77 \mu\text{m}$, SEM $\pm 6.05 \mu\text{m}$) showed a significant reduction in the mean total process length relative to controls ($M = 88.34 \mu\text{m}$, SEM $\pm 3.20 \mu\text{m}$), corresponding to an average of a 40.6 % reduction in total process length, $t(18) = 5.83$, $p < 0.01$. We next investigated the stress-induced changes in the process length within each of the 3- μm Sholl spheres across each of the four layers measured and found relative to controls, chronic stress was associated with a significant decrease in process length in layer II, $F(1, 18) = 22.58$, $p < 0.01$; layer III, $F(1, 18) = 8.55$, $p < 0.01$; layer V, $F(1, 18) = 16.63$, $p < 0.01$ and layer VI, $F(1, 18) = 43.28$, $p < 0.01$. Details regarding areas of statistical significance from planned comparisons are illustrated in Fig. 3.

Changes in the IL astrocyte process volume

Within each layer, process volume was initially assessed by calculating and comparing the volume of all cellular processes, and then further investigated by comparing the process volume within each of the concentric Sholl spheres. Irrespective of treatment condition, Sholl analysis showed that on average greater than 99 % of the total process volume was within 21 μm of the cell origin. Animals within the chronic stress condition ($M = 10.09 \mu\text{m}^3$, SEM $\pm 0.43 \mu\text{m}^3$) showed a significant reduction in the mean total volume relative to controls ($M = 17.97 \mu\text{m}^3$, SEM $\pm 1.14 \mu\text{m}^3$), corresponding to an average of a 56.0 % reduction in total process volume, $t(18) = 4.37$, $p < 0.01$. We next investigated the stress-induced changes in the process volume within each of the 3- μm Sholl spheres across each of the four layers measured and found relative to controls, chronic stress was associated with a significant decrease in cell volume in layer II, $F(1, 18) = 7.44$, $p < 0.02$; layer III, $F(1, 18) = 7.08$,

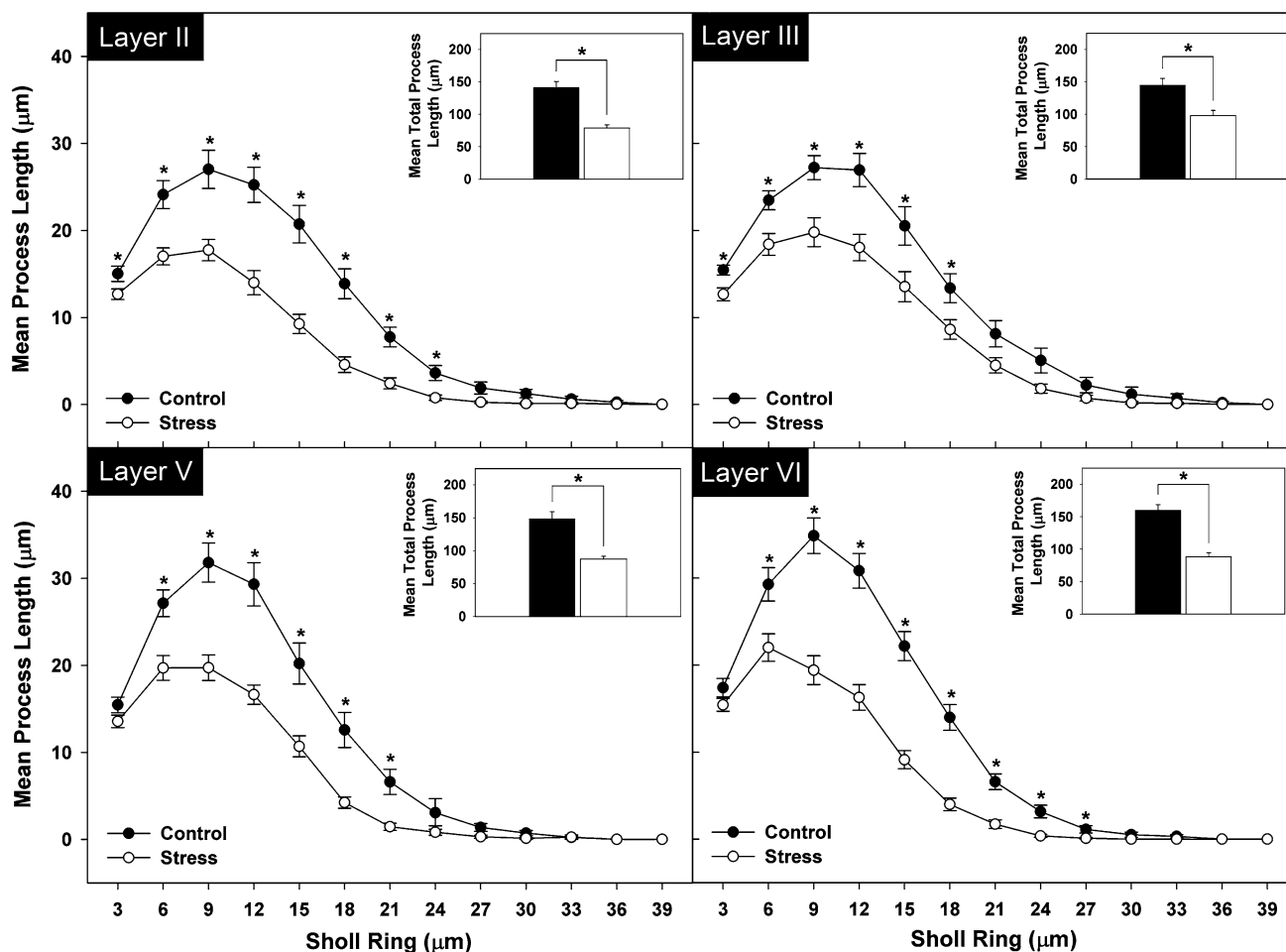


Fig. 3 Mean (\pm SEM) GFAP⁺ cellular process length of chronically stressed (white) and handled control (black) animals within each layer of the IL medial prefrontal cortex. Within each figure, the inset graph

shows the mean summation of process length from the entire cell. In all cases, asterisks indicate where planned comparisons indicated a significant difference ($p < 0.05$)

$p < 0.02$; layer V, $F(1, 18) = 7.98$, $p < 0.02$; and layer VI, $F(1, 18) = 37.54$, $p < 0.01$. Details regarding areas of statistical significance from planned comparisons are shown in Fig. 4.

Changes in the IL astrocyte branch number

Within each layer, the number of branches was assessed by calculating and comparing the number of bifurcating branch points, and then subsequently the number of bifurcations within each of the Sholl spheres measured. Irrespective of treatment condition, Sholl analysis indicated that bifurcations primarily occurred within the proximal aspect of the cell, with greater than 90 % of all branches occurring within 12 μ m of the cell origin. Animals exposed to chronic stress ($M = 4.94$, $SEM \pm 0.23$) showed a significant reduction in the mean number of branch points relative to controls ($M = 8.64$, $SEM \pm 0.36$), corresponding to an average of a 57.78 % reduction in the number of branch points,

$t(18) = 5.57$, $p < 0.01$. We next investigated the stress-induced changes in the branch points within each of the 3- μ m Sholl spheres across each of the four layers measured and found relative to controls, chronic stress was associated with a significant decrease in the number of branch points in layers II, $F(1, 18) = 20.77$, $p < 0.01$; layer III, $F(1, 18) = 6.41$, $p < 0.02$; layer V, $F(1, 18) = 20.32$, $p < 0.01$; and layer VI, $F(1, 18) = 53.78$, $p < 0.01$. Details regarding areas of statistical significance from planned comparisons are shown in Fig. 5.

Effects of chronic stress on GFAP immunolabelling

To verify consistency with existing literature, we sought to establish whether chronic stress influenced the total GFAP immunoreactivity within the IL PFC. This was evaluated over 2 rostrocaudal levels (+2.20 and +2.70 from Bregma), however, as there were no significant rostrocaudal differences (all $p > 0.05$), we report only group means

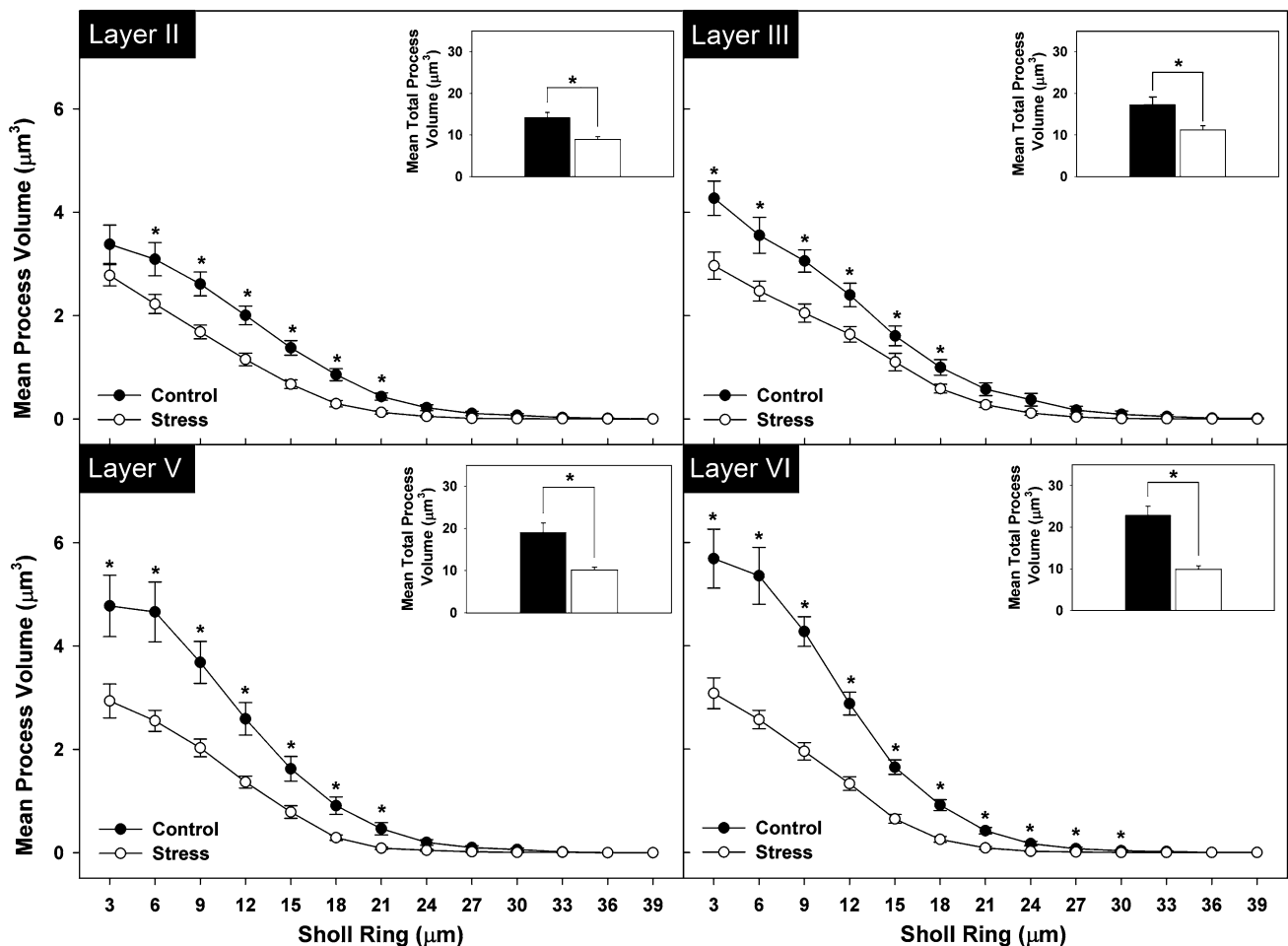


Fig. 4 Mean (\pm SEM) GFAP⁺ process volume of chronically stressed (white) and handled control (black) animals within each layer of the IL medial prefrontal cortex. Within each figure, the inset

graph shows the mean total process volume of the entire cell. In all cases, asterisks indicate where planned comparisons indicated a significant difference ($p < 0.05$)

that have been collapsed across the rostrocaudal levels. Data from the thresholded images of the total IL PFC indicated significantly greater density of immunoreactive material in the control sections ($M = 11.38\%$) when contrasted with stress tissue ($M = 7.06\%$), corresponding to an average of a 37.95% reduction in immunoreactive material, $t(18) = 4.95$, $p < 0.01$ (see Fig. 6). We then investigated the distribution of immunoreactive material, to determine if there were any differences in intensity as a function of layer in the IL PFC, and found a significant main effect of both layer, $F(4, 72) = 318.65$, $p < 0.01$, and experimental group, $F(1, 18) = 17.05$, $p < 0.01$, with a significant interaction between the two variables, $F(4, 72) = 10.11$, $p < 0.01$ (see Fig. 3). Tukey's post hoc analysis indicated that the difference in layers was driven by layer I, which had a greater density of immunoreactive material when contrasted with all other layers ($p < 0.05$), irrespective of treatment condition. Planned comparisons demonstrated that across all layers, control animals had

significantly greater intensity of immunoreactive material when contrasted with stressed animals (all $p < 0.05$; see Fig. 6). Finally, to assess the specificity of these observed changes, we also evaluated the density of immunoreactive material within the primary motor cortex, an area not commonly associated with stress, and found that there was no significant difference between controls and animals exposed to chronic stress in this region ($p > 0.05$).

Effects of chronic stress on the number of GFAP⁺ cells

The total number of GFAP⁺ astrocytes within the volume of IL PFC sampled was estimated using the optical fractionator method. The data indicated that within the overall IL PFC, there was a significant reduction in astrocyte number in animals exposed to chronic stress ($M = 7,360$, $SEM \pm 230$), when contrasted with the control condition ($M = 8,640$, $SEM \pm 328$), corresponding to an average of a 14.81% reduction in the total number of astrocytes,

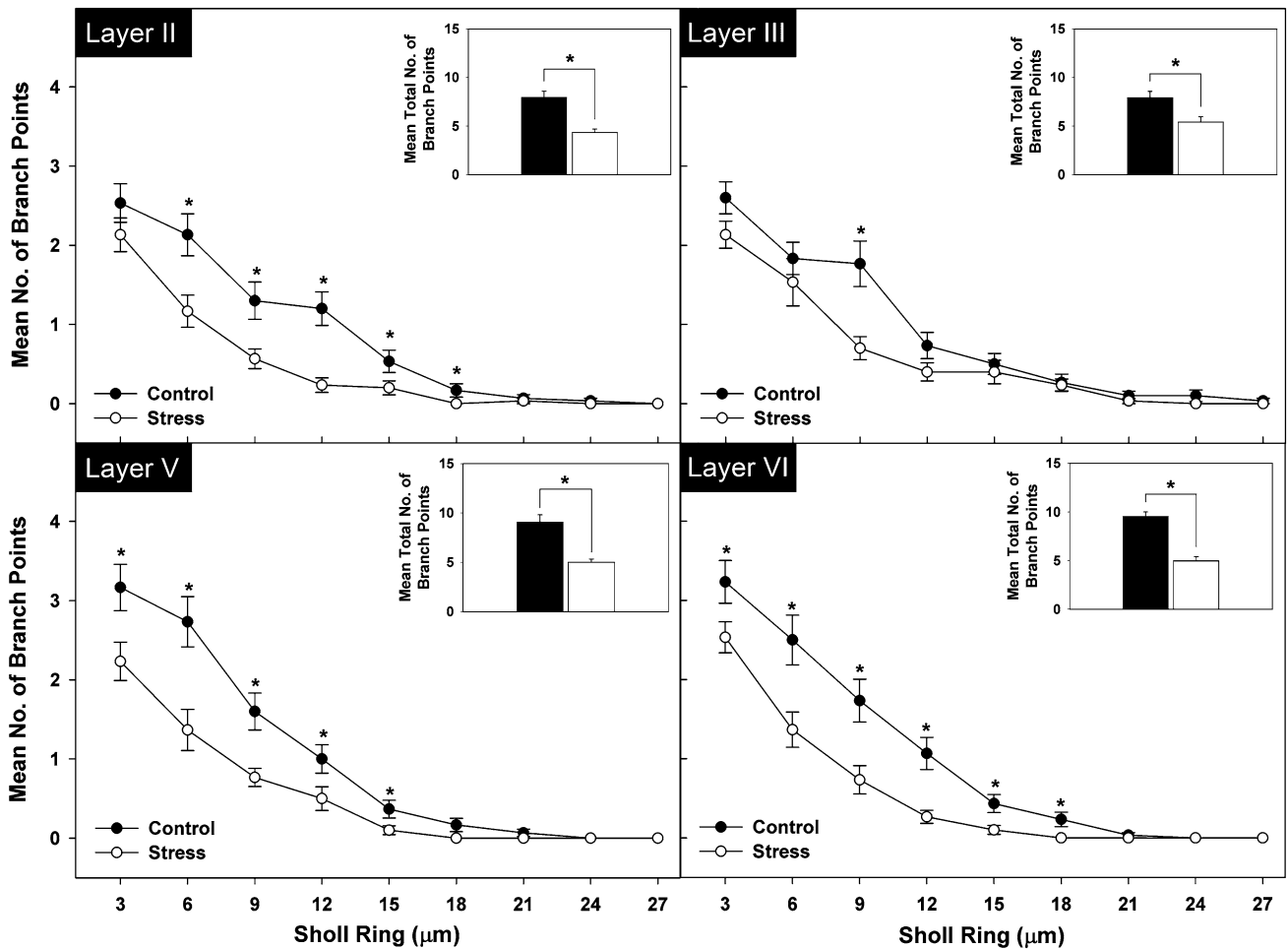
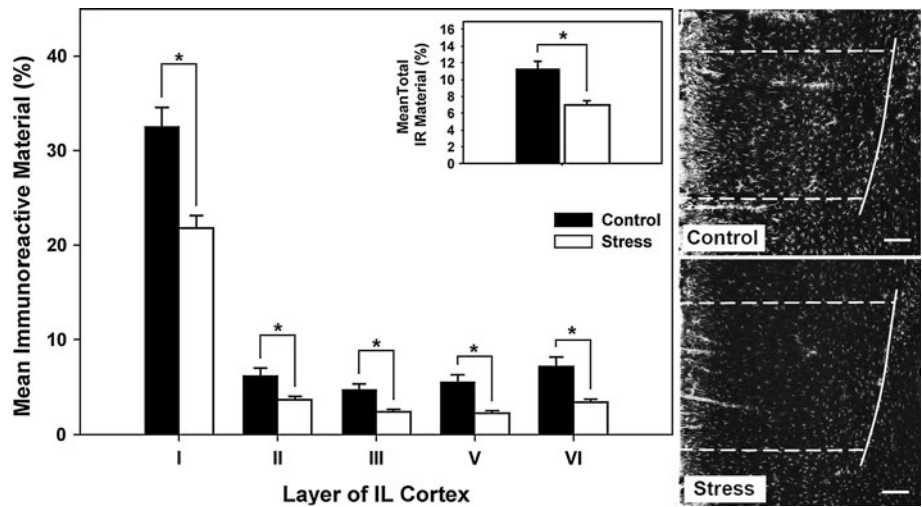


Fig. 5 Mean (±SEM) number of branch bifurcations in the GFAP⁺ cells of chronically stressed (white) and handled control (black) animals within each layer of the IL PFC. Within each figure, the inset

graph shows the average number of branch points in the entire cell for each layer. In all cases, asterisks indicate where planned comparisons indicated a significant difference ($p < 0.05$)

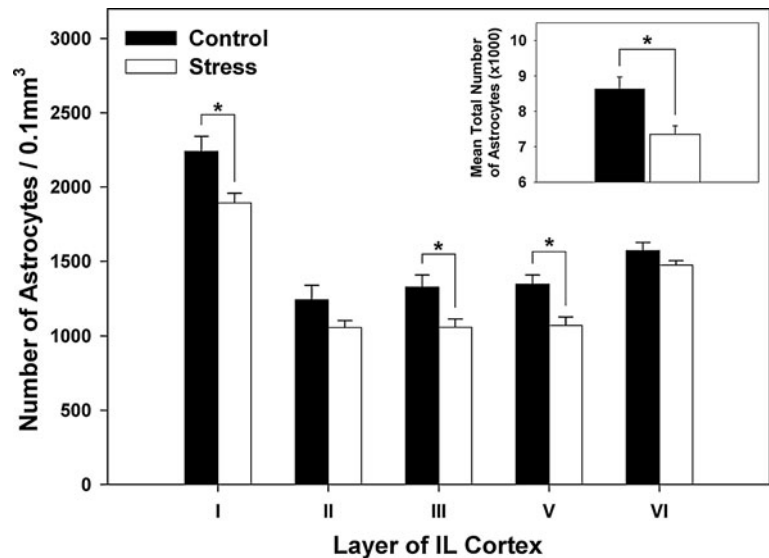
Fig. 6 Stress-induced reduction in the density of GFAP⁺ immunoreactive material within each layer of the IL PFC. The inset figure shows the mean percentage of immunoreactive material within the total IL PFC. Asterisks indicate area of statistical significance ($p < 0.05$). The photomicrographs represent typical imaging of GFAP-labelled tissue taken from the brain of control and chronically stress-treated rats, respectively. In both images, the anatomical location of the IL PFC is overlaid. Scale bar 200 µm



$t(16) = 2.94, p = 0.01$ (see Fig. 7). We next wanted to compare the cellular density within each layer, however, as the size and volume of each layer was not homogeneous,

we first transformed and normalized the estimated counts to determine the number of cells/0.1 mm³. From these transformations, we observed a significant main effect of

Fig. 7 Stress-induced reduction in the number of GFAP⁺ astrocytes within each layer of the IL PFC. The *inset figure* shows the estimated total number of astrocytes within the IL PFC, as determined using the optical fractionator counting method. Asterisks indicate area of statistical significance ($p < 0.05$)



both layer, $F(4, 64) = 113.55$, $p < 0.01$, and experimental group, $F(1, 16) = 8.13$, $p < 0.01$, but no significant interaction ($p > 0.05$). Tukey's post hoc analysis again indicated that the difference in layer was driven by a greater number of cells within layer I when contrasted with all other layers ($p < 0.01$), irrespective of treatment condition, with no significant within group differences in the other layers (all $p > 0.05$). Planned comparisons of between group differences indicated that the control group had a greater number of cells in layer I, $t(16) = 2.66$, $p = 0.017$; layer III, $t(16) = 2.48$, $p = 0.025$; and layer V, $t(16) = 3.050$, $p = 0.008$; with no significant differences in layer II or VI (in both cases $p > 0.05$; see Fig. 7).

Effect of chronic stress on the number of Nissl⁺ cells

We next investigated whether the observed reduction in the number of GFAP⁺ cells was accompanied by a corresponding decrease in the overall number of cells, as indicated by stereological counts of Nissl⁺-stained cells. Though GFAP⁺ cell numbers were decreased in the IL PFC after stress, total cell numbers remained unchanged when compared with control animals ($p > 0.05$; see Fig. 8).

Effect of chronic stress on the number of S100β⁺ cells

In order to investigate whether the decrease in GFAP⁺ cells without a concomitant loss of total cell numbers was due to a reduction in GFAP expression, an alternative marker was utilized for identification of astrocytes in the IL PFC. Cells positive for S100β were exhaustively counted across the entire IL PFC. No differences between stress and control groups were observed ($p > 0.05$) (See Fig. 8).

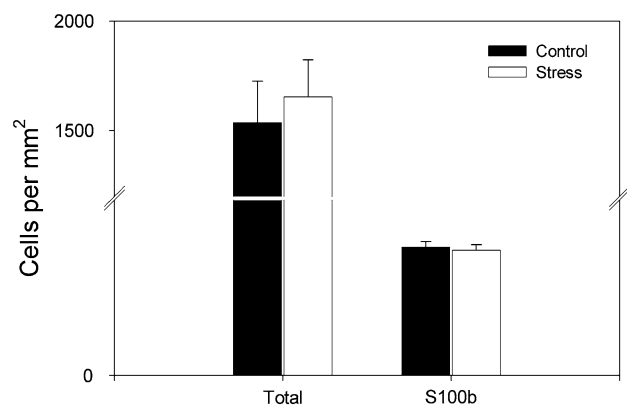
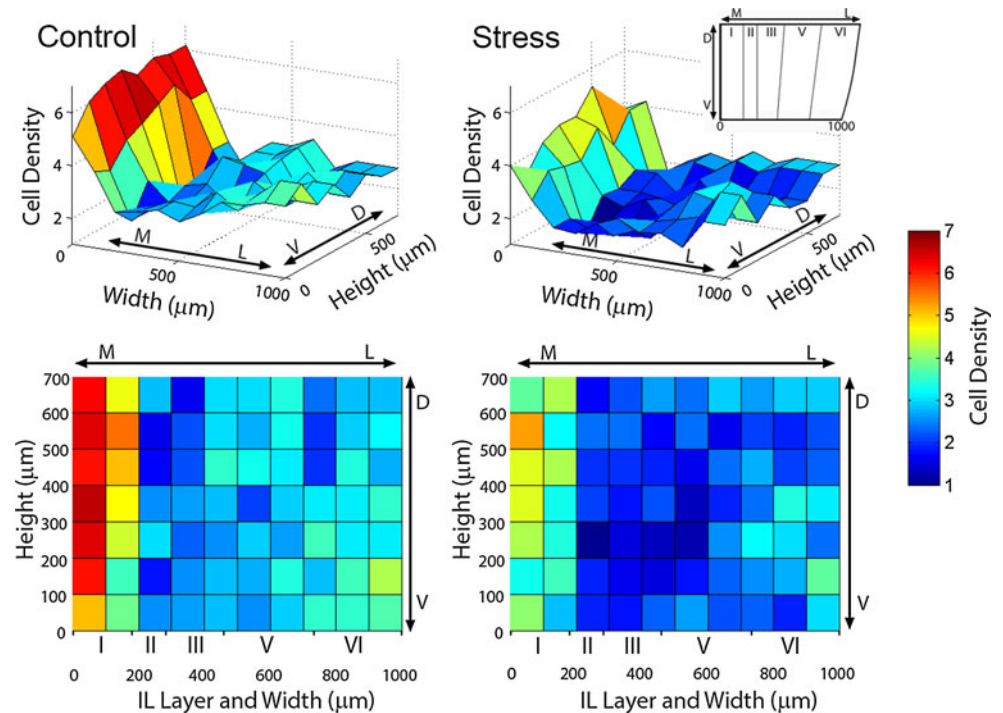


Fig. 8 Chronic stress did not change overall cell numbers in the IL PFC. A Nissl stain of all cells in the mPFC demonstrated no difference in cell numbers between control (black) and stress (white) groups. Cells positively stained for the astrocyte marker S100β also demonstrated no difference in population of the IL PFC. Values are expressed as \pm SEM

Effect of chronic stress on the distribution of GFAP⁺ cells

We next investigated how chronic stress influenced the distribution of GFAP⁺ astrocytes within the IL PFC. Precise XY co-ordinates of all cells within the IL PFC were extracted from GFAP-immunolabeled tissue and were used to generate a heatmap of the cellular density (see Fig. 9). These figures clearly illustrate the nature of the stress-induced reduction in the density of cells as revealed by both our thresholding and stereological assessments. We then compared the density of cells in the dorsal and ventral aspects of each cortical layer by determining within group, within layer differences. This analysis indicated that there was a significantly greater density of cells within the dorsal region of layer VI in animals exposed to chronic stress, $t(18) = 2.41$,

Fig. 9 Heatmaps illustrating the density of GFAP⁺ cells within the IL PFC of both stress and control animals in both 3D (upper panels) and 2D (lower panels). The scale bar on the right indicates the density of cells within each square cell of the heat map grid. *M* medial, *L* lateral, *D* dorsal, *V* ventral



$p = 0.029$, with no significant within layer differences for all other cortical layers measured. This result indicates that while there was a stress-induced overall decrease in the density of cells, the proportionate distribution of cells within each layer was minimally influenced by stress exposure.

Intra- and extrasomal intensity of S100 β

As cellular atrophy is often indicative of cell distress, we investigated chronic stress-induced changes in the intra- and extrasomal expressions of S100 β , a protein marker commonly associated with astrocyte stress. A general increase in both the intra- and extrasomal expressions of S100 β was noted (Fig. 10a, b). When individual astrocytes from each group were ranked in order of S100 β intensity, astrocytes from chronically stressed rats nearly always displayed greater S100 β than their matched controls. However, our results indicated that relative to controls, chronic stress was associated with significant elevations in extrasomal [$t(18) = -3.25, p < 0.01$] but not intrasomal [$t(15) = -0.92, p > 0.05$] expression of S100 β (Fig. 10c, d). In addition, no correlation between intra- and extrasomal levels of S100 β and astrocyte morphology was observed, suggesting that S100 β expression was increased independently of structural changes to PFC astrocytes.

Discussion

One of the most consistently identified environmental challenges recognized to disrupt PFC function is exposure

to chronic stress [3, 21]. At a cellular level, the ability of stress to induce profound structural remodelling of neurons is well described [41, 43, 44, 53]. By comparison, much less is known about how chronic stress alters astrocytes within the PFC. In an effort to further our understanding of how astrocytes are altered by stress, we undertook a detailed neuroanatomical investigation to determine whether exposure to chronic stress could induce significant structural remodelling of astrocytes within the PFC. To investigate this question, we digitally reconstructed astrocytes using high-resolution three-dimensional images acquired using confocal laser scanning microscopy. The results from this research have revealed that astrocytes undergo profound structural remodelling, consistent with atrophy, as a result of exposure to chronic stress.

Using a label specific to the astrocyte protein GFAP, our analysis revealed that chronic stress produced a substantial decrease in three main morphological parameters of astrocytes, with an average of a $\sim 40\%$ reduction in process length, a $\sim 56\%$ decrease in process volume, and a $\sim 58\%$ decline in the number of process branches. Across each of the cortical layers examined, our analysis of these changes indicated that the magnitude of change was remarkably consistent. To our knowledge, this is the first demonstration of structural remodelling of astrocytes following exposure to chronic stress. Therefore, it is only possible to speculate about the overall significance of these findings. Nevertheless, given the profound level of atrophy, that the effect appears to be region-wide, and the recognized involvement of astrocytic processes in regulating

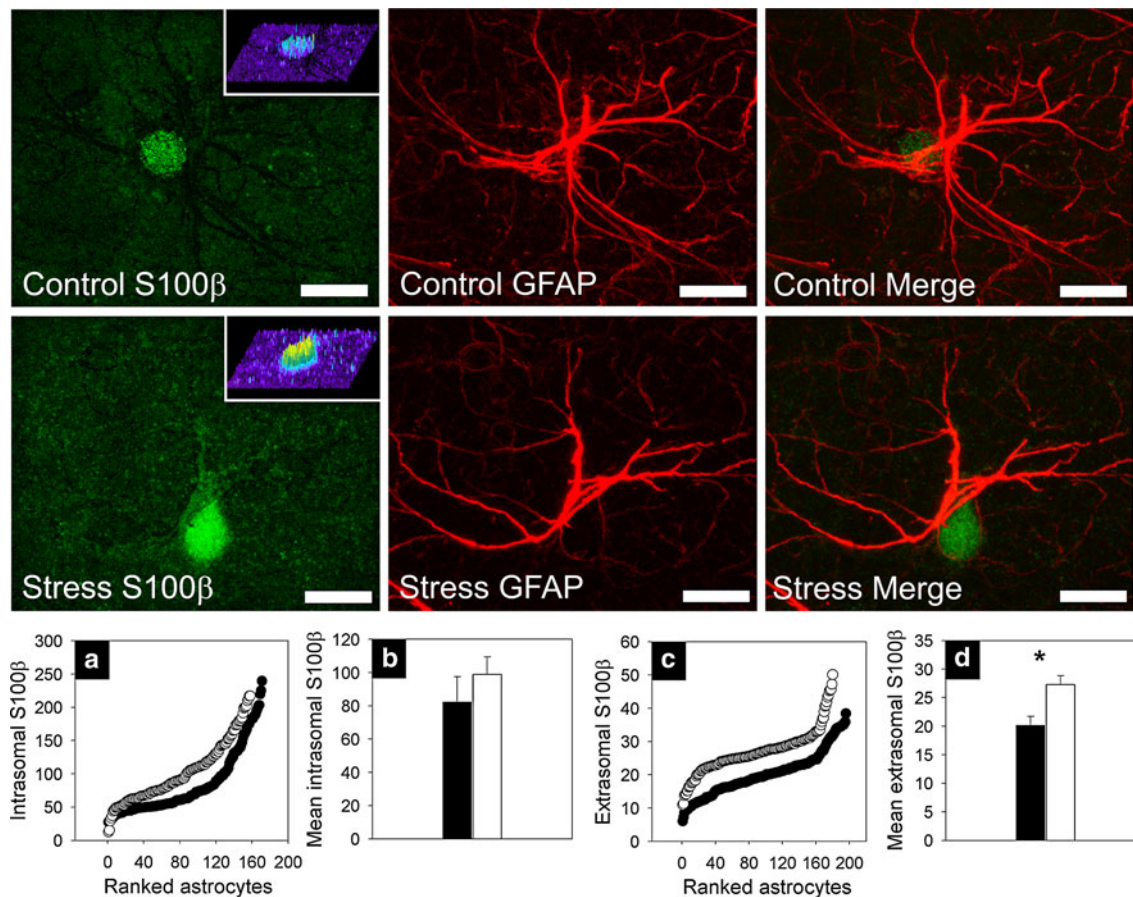


Fig. 10 Co-localization of GFAP and astrocyte-specific S100 β immunoreactive material. The *upper panel of photomicrographs* represents maximum intensity projections of confocal image stacks taken from both control- (*upper row*) and stress-treated (*lower row*) rats. The tissue was co-labelled with S100 β (*left*) and GFAP (*centre*), with a corresponding merge of the two images (*right*) illustrating a significant degree of co-localization. Within each of the S100 β images, the *inset figure* shows a colour intensity profile for intra- and extranasal S100 β for the pictured astrocyte. Higher colour intensity

synaptic function, the influence could be considerable. Certainly, this result is complementary to existing knowledge concerning GFAP⁺ cell loss within the PFC and goes some way to providing a clearer picture of how chronic stress disrupts PFC function [9, 12, 62].

Previous findings have consistently reported the ability of chronic stress to reduce the number of GFAP⁺ cells [22, 47]. Therefore, it was of great interest to determine whether the stress protocol we used in the current study also produced these effects. Accordingly, we undertook several assessments examining changes in both GFAP⁺ immunoreactivity and the density of GFAP⁺ cells. In addition to these assessments, we also evaluated changes in cell density using two GFAP-independent methods. We undertook these latter procedures as there has been some research to suggest that GFAP expression can vary in a manner that is not dependent upon the viability of the cells, leading to a

situation where GFAP-based stereological assessment may not provide a totally accurate estimate of changes in cell number [7, 23, 54].

In terms of the GFAP-dependent methods, we used both thresholding and unbiased stereological counting to quantify astrocytes. Consistent with previous findings [22, 47], the results of the thresholding analysis revealed that chronic stress induced a significant reduction in the quantity of GFAP immunoreactive labelling (~38%). Similarly, the results from our unbiased stereological assessment confirmed existing findings regarding a chronic stress-induced global reduction in the number of GFAP⁺ cells within the PFC [30]. Of note, these alterations appear to be reasonably circuit specific, as we could not find any evidence of equivalent alterations within the motor cortex, an area not traditionally recognized to be disturbed by exposure to chronic stress.

Exhaustive counting of GFAP⁺ cells across cortical layers indicated that irrespective of treatment, there was a significantly greater density of GFAP cells within layer I, with no difference in the density between all subsequent layers, giving rise to the characteristic L shape observed in the three-dimensional heat maps. When we evaluated the laminar distribution of GFAP⁺ cells, we found that the number of cells within each layer was homogenous, with few significant differences in density between the dorsal and ventral portions of each layer for either treatment condition. After chronic stress treatment, a region-wide decrease in the density of immunoreactive material across each of the cortical layers was revealed by our thresholding analysis. However, the results from our unbiased stereological analysis of cellular density indicated that statistically, reductions were only significant in layers I, III and V, with no significant change in either layer II or VI.

While the current study is the first, to our knowledge, to examine astrocyte remodelling following chronic stress, other research groups have identified similar changes in astrocyte density. Specifically, Banasr and Duman [4], using unbiased stereological assessment, demonstrated that chronic unpredictable mild stress significantly decreased the number of GFAP⁺ astrocytes within the PFC. These results also align with a decrease in GFAP⁺ cells reported to occur in the hippocampus [13]. Among the few other studies to have systematically quantified chronic stress-induced changes in astrocytes, Ye et al. [61] found a significant decrease in GFAP protein within the hippocampus using Western blot analysis; and Imbe et al. [30], using a thresholding approach, showed a stress-induced decrease in GFAP immunoreactive material in the periaqueductal grey. Based on this literature, several groups have proposed that the reduced number of astrocytes is directly linked to disruptions in cognitive behaviour, with many now focused on astrocyte loss as a primary driver of pathology [6]. Indeed, this proposal seems to be empirically well supported by the study of Banasr and Duman [5] who demonstrated that the application of the astrocyte specific toxin L-alpha-aminodipic resulted in astrocyte ablation within the PFC, and was sufficient to induce depressive-like behaviour, similar to that observed following exposure to chronic stress.

To confirm our finding that chronic stress had decreased the number of astrocytes within the PFC, we also assessed changes in cell density using GFAP-independent measurements. We utilized Nissl staining as our primary GFAP-independent method. The Nissl stain binds extra nuclear RNA, making it a ubiquitous and highly utilized approach for assessing changes in cell density [20, 40]. Interestingly, our assessment of cell density within the PFC using Nissl-based stereological counting indicated that there were no statistical differences between the density of cells in the stress and control groups. However, as Nissl

stain is a non-specific cellular marker, it cannot be readily used to distinguish between neurons and different types of glia. Accordingly, it is possible that chronic stress reduced the number of astrocytes but caused a corresponding increase in another cell type. While a remote possibility, this consideration led us to undertake a count of S100 β , which has frequently been used as a marker of mature astrocytes. As was the case with the Nissl counts, we could not find any statistical difference in the number of S100 β ⁺ cells within the PFC between the stress and control groups. Together, this set of results suggests that chronic stress, using the 21-day restraint stress model, does not reduce the numbers of astrocytes. A more likely scenario is that chronic stress reduces the expression of GFAP.

The ability of chronic stress to decrease GFAP expression but not astrocyte numbers helps resolve a long-standing paradox; specifically, evidence demonstrating the absence of a neuroinflammatory response in chronically stressed animals [26, 57]. To elaborate, if it was the case that chronic stress actually caused a 15–20 % reduction in the number of astrocytes, one may anticipate a robust inflammatory response within the same region. Previously, however, we have determined, using a model identical to that reported in the current study, that chronic stress did not cause an appreciable increase in the pro-inflammatory cytokine interleukin-1 β ; did not increase the expression of the antigen presentation marker MHC-II; did not increase the expression of CD68, a marker of microglial phagocytosis; nor did it increase the expression of apoptotic markers (activated caspase-3 or TUNEL) [27]. Moreover, microglia within the PFC became hyper-ramified rather than assuming a hypo-ramified state, which is associated with the pro-inflammatory state induced by injury [27]. These results which indicate that there is a negligible neuroinflammatory response within the PFC of stress animals interdigitates extremely well with the present finding that there is no major loss of cells within the PFC following stress.

For some time now, GFAP has been the most extensively used marker to identify astrocytes [11, 15, 22, 30]. Specifically, it identifies the intermediate filaments that comprise the cell's cytoskeleton [55]. Whilst this feature makes GFAP an extremely useful and appropriate marker to investigate structural remodelling, it was clear that the immunolabelling and imaging procedure used in the current study did not perfectly resolve extremely fine GFAP⁺ processes. It may be possible to circumvent this issue using an approach such as stimulated emission depletion microscopy to achieve higher spatial resolution. Nevertheless, it is likely to be the case that our investigative approach has provided an underestimate of the real magnitude of stress-induced cytoskeletal atrophy. It is also important to draw attention to the fact that GFAP labelling

only identifies one aspect of the cell's overall structure. Indeed, it is estimated that GFAP only accounts for approximately 15 % of the astrocyte's overall volume [10]. Accordingly, it is worthwhile to note that no definitive generalizations can be made with respect to changes in cytoskeleton to changes in the overall volume of the cell. It would, nevertheless, seem reasonable to hypothesize that the cytoskeleton and the overall area occupied by the cell within the central nervous system would be highly correlated.

In terms of understanding the changes induced by chronic stress, one of the most consistent findings has been the pronounced dendritic atrophy and dendritic spine loss within layers II/III of the PFC [31, 41, 48, 53]. These findings appear to be highly consistent with a raft of clinical imaging studies, which have consistently demonstrated that individuals with a significant life history of depression exhibit marked reductions in grey matter volume within the ventromedial PFC [16, 37]. While many have hypothesized that it is these neuronal alterations that contribute to the emergence of cognitive and mood disturbances seen in individuals exposed to chronic stress [17], the specific mechanisms that contribute to these neuronal changes have remained elusive. However, studies over the past several years have strongly suggested that disturbances in astrocytes may play a role in stress induced neuronal and cognitive disturbances [18].

Over the past decade, several research groups have provided evidence that astrocytes may play a central role in mediating the effects of stress on neuronal structure and function [12, 22, 47, 51]. Based on the available evidence, it had become widely accepted that chronic stress induced a significant reduction in astrocyte density and that this reduction was pivotal to the observed neuronal disturbances. Contrary to this established understanding, the results from the current study suggest that chronic stress may not induce a reduction in astrocyte numbers, but rather significantly lower the expression of the GFAP marker upon which prior density assessments have been predicated. The fact that astrocytes are not dying should not, however, be taken to indicate that there are not profound changes in this cell group. Indeed, in the present study we have provided evidence demonstrating that chronic stress results in widespread structural atrophy of the astrocyte. This atrophy is likely to be extremely important given that GFAP is a major cytoskeletal protein that facilitates the astrocytes ability to appropriately remodel itself in response to environmental signals [49, 55].

One intriguing candidate mechanism that may have contributed to the remodelling of astrocytes is S100 β , a protein that is particularly concentrated within astrocytes. Elevated levels of S100 β have been widely recognized in association with astrocyte distress [28]. However, recent

observations suggest a much more sophisticated concentration-dependent role for this calcium binding globulin. For instance, at nanomolar concentrations, S100 β has been shown to possess neurotrophic qualities, promoting neurogenesis, cell survival, growth and differentiation [29, 58]. Micromolar concentrations of S100 β , however, have been associated with both glial and neuronal apoptosis, as a consequence of S100 β -induced up-regulation of cyclooxygenase-2 and elevations in free radical release [8, 28, 29]. Accordingly, from a theoretical perspective, alterations in the expression of S100 β represent a plausible pathway that may contribute to the observed changes in astrocytes. In the current study, we observed that extrasomal but not intrasomal S100 β was elevated within the PFC following exposure to chronic stress. These observed results align well with clinical research demonstrating elevated serum levels of S100 β in individuals suffering from major depression [51, 52] and from one other study that has examined S100 β in hippocampal homogenate [61]. Given the deleterious effects attributed to high levels of S100 β , it was of interest that our analysis revealed that there was no significant relationship between levels of S100 β and astrocyte remodelling. These results suggest that the mechanisms responsible for the structural atrophy of astrocytes are separate to those responsible for increasing S100 β expression.

Clearly, identifying the signalling molecules responsible for driving astrocyte atrophy is now an issue of considerable interest. In the current study, we hypothesized that S100 β may contribute to cellular atrophy, given that the protein is known to be released by astrocytes and has been found to be elevated in patients with depression. While we found exposure to chronic stress increased S100 β within the PFC, we could find no statistical evidence of a relationship with astrocyte remodelling.

When the results of the current study are taken in conjunction with earlier work on microglia, it appears that chronic stress can exert a very significant influence on glial morphology. Specifically, chronic stress, at least within the PFC, appears to promote microglial hyper-ramification and astroglial atrophy. At this stage we can only speculate on what the broader significance of these remodelling events may be. Recently, however, it is been recognized that astrocytes and microglia have an important contribution to synaptic function. Indeed, it is recently been suggested that the concept of the synapse be expanded (the quadripartite synapse) to acknowledge the central role of both astrocytes and microglia to synaptic function [24, 56]. Although much more experimental work lies ahead to explore this concept, it is intriguing to consider the possibility that chronic stress influences neuronal function by disrupting glial interactions at the level of the synapse. Finally, the results from the current study call attention to the fact that strategies

directed towards mitigating stress-induced cognitive impairments may prove to be more therapeutically effective if they also take into consideration their ability to reconsolidate pre-stress glial structure. In summary, the current findings concerning structural atrophy of astrocytes, in conjunction with their known role in modulating synaptic function, may help explain why chronic stress can provoke substantial changes in cognitive behaviour and mood state.

Acknowledgments These studies were supported by funding from the Australian National Health and Medical Research Council, the Hunter Medical Research Institute, and the University of Newcastle's Centre for Translational Neuroscience and Mental Health Research.

References

- Anderson CM, Swanson RA (2000) Astrocyte glutamate transport: review of properties, regulation, and physiological functions. *Glia* 32:1–14
- Andreazza AC, Cassini C, Rosa AR et al (2007) Serum S100B and antioxidant enzymes in bipolar patients. *J Psychiatr Res* 41:523–529. doi:10.1016/j.jpsychires.2006.07.013
- Arnsten AF (2009) Stress signalling pathways that impair prefrontal cortex structure and function. *Nat Rev Neurosci* 10:410–422. doi:10.1038/nrn2648
- Banasr M, Duman RS (2007) Regulation of neurogenesis and gliogenesis by stress and antidepressant treatment. *CNS Neurol Disord Drug Targets* 6:311–320
- Banasr M, Duman RS (2008) Keeping 'trk' of antidepressant actions. *Neuron* 59:349–351. doi:10.1016/j.neuron.2008.07.028
- Banasr M, Dwyer JM, Duman RS (2011) Cell atrophy and loss in depression: reversal by antidepressant treatment. *Curr Opin Cell Biol* 23:730–737. doi:10.1016/j.ceb.2011.09.002
- Beynon SB, Walker FR (2012) Microglial activation in the injured and healthy brain: what are we really talking about? Practical and theoretical issues associated with the measurement of changes in microglial morphology. *Neuroscience* 225:162–171. doi:10.1016/j.neuroscience.2012.07.029
- Bianchi R, Giambanco I, Donato R (2010) S100B/RAGE-dependent activation of microglia via NF-kappaB and AP-1 Co-regulation of COX-2 expression by S100B, IL-1beta and TNF-alpha. *Neurobiol Aging* 31:665–677. doi:10.1016/j.neurobiolaging.2008.05.017
- Broe M, Kril J, Halliday GM (2004) Astrocytic degeneration relates to the severity of disease in frontotemporal dementia. *Brain* 127:2214–2220. doi:10.1093/brain/awh250
- Bushong EA, Martone ME, Jones YZ, Ellisman MH (2002) Protoplasmic astrocytes in CA1 stratum radiatum occupy separate anatomical domains. *J Neurosci* 22:183–192
- Corvetto L, Capsoni S, Cattaneo A, Domenici L (2003) Postnatal development of GFAP in mouse visual cortex is not affected by light deprivation. *Glia* 41:404–414
- Cotter DR, Pariante CM, Everall IP (2001) Glial cell abnormalities in major psychiatric disorders: the evidence and implications. *Brain Res Bull* 55:585–595
- Czeh B, Simon M, Schmelting B, Hiemke C, Fuchs E (2006) Astroglial plasticity in the hippocampus is affected by chronic psychosocial stress and concomitant fluoxetine treatment. *Neuropsychopharmacology* 31:1616–1626. doi:10.1038/sj.npp.1300982
- Ding DC, Gabbott PL, Totterdell S (2001) Differences in the laminar origin of projections from the medial prefrontal cortex to the nucleus accumbens shell and core regions in the rat. *Brain Res* 917:81–89
- Drage MG, Holmes GL, Seyfried TN (2002) Hippocampal neurons and glia in epileptic EL mice. *J Neurocytol* 31:681–692
- Drevets WC, Price JL, Simpson JR Jr et al (1997) Subgenual prefrontal cortex abnormalities in mood disorders. *Nature* 386:824–827. doi:10.1038/386824a0
- Drevets WC, Price JL, Furey ML (2008) Brain structural and functional abnormalities in mood disorders: implications for neurocircuitry models of depression. *Brain Struct Funct* 213:93–118. doi:10.1007/s00429-008-0189-x
- Eyre H, Baune BT (2012) Neuroplastic changes in depression: a role for the immune system. *Psychoneuroendocrinology*. doi:10.1016/j.psyneuen.2012.03.019
- Gabbott PL, Warner TA, Jays PR, Salway P, Busby SJ (2005) Prefrontal cortex in the rat: projections to subcortical autonomic, motor, and limbic centers. *J Comp Neurol* 492:145–177. doi:10.1002/cne.20738
- Garcia-Amado M, Prensa L (2012) Stereological analysis of neuron, glial and endothelial cell numbers in the human amygdaloid complex. *PLoS One* 7:e38692. doi:10.1371/journal.pone.0038692
- Goldwater DS, Pavlides C, Hunter RG et al (2009) Structural and functional alterations to rat medial prefrontal cortex following chronic restraint stress and recovery. *Neuroscience* 164:798–808
- Gosselin RD, Gibney S, O'Malley D, Dinan TG, Cryan JF (2009) Region specific decrease in glial fibrillary acidic protein immunoreactivity in the brain of a rat model of depression. *Neuroscience* 159:915–925. doi:10.1016/j.neuroscience.2008.10.018
- Guidry C, King JL, Mason JO 3rd (2009) Fibrocontractive Muller cell phenotypes in proliferative diabetic retinopathy. *Invest Ophthalmol Vis Sci* 50:1929–1939. doi:10.1167/iovs.08-2475
- Schafer DP, Lehrman EK, Stevens B (2013) The "quad-partite" synapse: microglia–synapse interactions in the developing and mature CNS. *Glia* 61(1):24–36. doi:10.1002/glia.22389 (Epub 2012 Jul 24)
- Hammen C (2005) Stress and depression. *Annu Rev Clin Psychol* 1:293–319
- Hinwood M, Morandini J, Day TA, Walker FR (2012) Evidence that microglia mediate the neurobiological effects of chronic psychological stress on the medial prefrontal cortex. *Cereb Cortex* 22:1442–1454. doi:10.1093/cercor/bhr229
- Hinwood M, Tynan RJ, Charnley JL, Beynon SB, Day TA, Walker FR (2012) Chronic Stress Induced Remodeling of the Prefrontal Cortex: Structural Re-Organization of Microglia and the Inhibitory Effect of Minocycline. *Cereb Cortex*. doi:10.1093/cercor/bhs151
- Hu J, Van Eldik LJ (1996) S100 beta induces apoptotic cell death in cultured astrocytes via a nitric oxide-dependent pathway. *Biochim Biophys Acta* 1313:239–245
- Huttunen HJ, Kuja-Panula J, Sorci G, Agneletti AL, Donato R, Rauvala H (2000) Coregulation of neurite outgrowth and cell survival by amphotericin and S100 proteins through receptor for advanced glycation end products (RAGE) activation. *J Biol Chem* 275:40096–40105. doi:10.1074/jbc.M006993200
- Imbe H, Kimura A, Donishi T, Kaneoke Y (2012) Chronic restraint stress decreases glial fibrillary acidic protein and glutamate transporter in the periaqueductal gray matter. *Neuroscience* 223:209–218. doi:10.1016/j.neuroscience.2012.08.007
- Izquierdo A, Wellman CL, Holmes A (2006) Brief uncontrollable stress causes dendritic retraction in infralimbic cortex and resistance to fear extinction in mice. *J Neurosci* 26:5733–5738. doi:10.1523/JNEUROSCI.0474-06.2006
- Jinno S, Fleischer F, Eckel S, Schmidt V, Kosaka T (2007) Spatial arrangement of microglia in the mouse hippocampus: a

- stereological study in comparison with astrocytes. *Glia* 55: 1334–1347
33. Kreutzberg GW (1996) Microglia: a sensor for pathological events in the CNS. *Trends Neurosci* 19:312–318. doi:[10.1016/0166223696100497](https://doi.org/10.1016/0166223696100497)
 34. Michetti F, Corvino V, Geloso MC et al (2012) The S100B protein in biological fluids: more than a lifelong biomarker of brain distress. *J Neurochem* 120:644–659. doi:[10.1111/j.1471-4159.2011.07612.x](https://doi.org/10.1111/j.1471-4159.2011.07612.x)
 35. Montgomery DL (1994) Astrocytes: form, functions, and roles in disease. *Vet Pathol* 31:145–167
 36. Morshedi MM, Meredith GE (2007) Differential laminar effects of amphetamine on prefrontal parvalbumin interneurons. *Neuroscience* 149:617–624. doi:[10.1016/j.neuroscience.2007.07.047](https://doi.org/10.1016/j.neuroscience.2007.07.047)
 37. Ongur D, Drevets WC, Price JL (1998) Glial reduction in the subgenual prefrontal cortex in mood disorders. *Proc Natl Acad Sci USA* 95:13290–13295
 38. Paxinos G, Watson C (1998) *The rat brain in stereotaxic coordinates*. Academic Press, Waltham
 39. Petzold A, Eikelenboom MJ, Gveric D et al (2002) Markers for different glial cell responses in multiple sclerosis: clinical and pathological correlations. *Brain* 125:1462–1473
 40. Pilati N, Barker M, Panteleimonitis S, Donga R, Hamann M (2008) A rapid method combining Golgi and Nissl staining to study neuronal morphology and cytoarchitecture. *J Histochem Cytochem* 56:539–550. doi:[10.1369/jhc.2008.950246](https://doi.org/10.1369/jhc.2008.950246)
 41. Radley JJ, Sisti HM, Hao J et al (2004) Chronic behavioral stress induces apical dendritic reorganization in pyramidal neurons of the medial prefrontal cortex. *Neuroscience* 125:1–6
 42. Radley JJ, Arias CM, Sawchenko PE (2006) Regional differentiation of the medial prefrontal cortex in regulating adaptive responses to acute emotional stress. *J Neurosci* 26:12967–12976. doi:[10.1523/JNEUROSCI.4297-06.2006](https://doi.org/10.1523/JNEUROSCI.4297-06.2006)
 43. Radley JJ, Rocher AB, Miller M et al (2006) Repeated stress induces dendritic spine loss in the rat medial prefrontal cortex. *Cereb Cortex* 16:313–320. doi:[10.1093/cercor/bhi104](https://doi.org/10.1093/cercor/bhi104)
 44. Radley JJ, Rocher AB, Rodriguez A et al (2008) Repeated stress alters dendritic spine morphology in the rat medial prefrontal cortex. *J Comp Neurol* 507:1141–1150. doi:[10.1002/cne.21588](https://doi.org/10.1002/cne.21588)
 45. Rajkowska G (2000) Histopathology of the prefrontal cortex in major depression: what does it tell us about dysfunctional monoaminergic circuits? *Prog Brain Res* 126:397–412. doi:[10.1016/S0079-6123\(00\)26026-3](https://doi.org/10.1016/S0079-6123(00)26026-3)
 46. Rajkowska G (2002) Cell pathology in mood disorders. *Semin Clin Neuropsychiatry* 7:281–292
 47. Rajkowska G, Miguel-Hidalgo JJ (2007) Gliogenesis and glial pathology in depression. *CNS Neurol Disord Drug Targets* 6:219–233
 48. Ramkumar K, Srikumar BN, Venkatasubramanian D, Siva R, Shankaranarayana Rao BS, Raju TR (2012) Reversal of stress-induced dendritic atrophy in the prefrontal cortex by intracranial self-stimulation. *J Neural Transm* 119:533–543. doi:[10.1007/s00702-011-0740-4](https://doi.org/10.1007/s00702-011-0740-4)
 49. Saur L, Baptista PP, de Senna PN et al (2013) Physical exercise increases GFAP expression and induces morphological changes in hippocampal astrocytes. *Brain Struct Funct*. doi:[10.1007/s00429-012-0500-8](https://doi.org/10.1007/s00429-012-0500-8)
 50. Savchenko VL, McKanna JA, Nikonenko IR, Skibo GG (2000) Microglia and astrocytes in the adult rat brain: comparative immunocytochemical analysis demonstrates the efficacy of lipocortin 1 immunoreactivity. *Neuroscience* 96:195–203
 51. Schroeter ML, Abdul-Khaliq H, Krebs M, Diefenbacher A, Blasig IE (2008) Serum markers support disease-specific glial pathology in major depression. *J Affect Disord* 111:271–280. doi:[10.1016/j.jad.2008.03.005](https://doi.org/10.1016/j.jad.2008.03.005)
 52. Schroeter ML, Steiner J, Mueller K (2011) Glial pathology is modified by age in mood disorders—a systematic meta-analysis of serum S100B in vivo studies. *J Affect Disord* 134:32–38. doi:[10.1016/j.jad.2010.11.008](https://doi.org/10.1016/j.jad.2010.11.008)
 53. Shansky RM, Hamo C, Hof PR, McEwen BS, Morrison JH (2009) Stress-induced dendritic remodeling in the prefrontal cortex is circuit specific. *Cereb Cortex* 19:2479–2484. doi:[10.1093/cercor/bhp003](https://doi.org/10.1093/cercor/bhp003)
 54. Sofroniew MV, Vinters HV (2010) Astrocytes: biology and pathology. *Acta Neuropathol* 119:7–35. doi:[10.1007/s00401-009-0619-8](https://doi.org/10.1007/s00401-009-0619-8)
 55. Sotelo J, Toh BH, Lolait SJ, Yildiz A, Osung O, Holborow EJ (1980) Cytoplasmic intermediate filaments in cultured glial cells. *Neuropathol Appl Neurobiol* 6:291–298
 56. Tremblay ME, Majewska AK (2011) A role for microglia in synaptic plasticity? *Commun Integr Biol* 4:220–222. doi:[10.4161/cib.4.2.14506](https://doi.org/10.4161/cib.4.2.14506)
 57. Tynan RJ, Naicker S, Hinwood M et al (2010) Chronic stress alters the density and morphology of microglia in a subset of stress-responsive brain regions. *Brain Behav Immun* 24:1058–1068. doi:[10.1016/j.bbi.2010.02.001](https://doi.org/10.1016/j.bbi.2010.02.001)
 58. Van Eldik LJ, Griffin WS (1994) S100 beta expression in Alzheimer's disease: relation to neuropathology in brain regions. *Biochim Biophys Acta* 1223:398–403
 59. Wearne SL, Rodriguez A, Ehlenberger DB, Rocher AB, Henderson SC, Hof PR (2005) New techniques for imaging, digitization and analysis of three-dimensional neural morphology on multiple scales. *Neuroscience* 136:661–680. doi:[10.1016/j.neuroscience.2005.05.053](https://doi.org/10.1016/j.neuroscience.2005.05.053)
 60. Yang CY, Matsuzaki T, Iijima N, Kajimura N, Ozawa H (2012) Morphofunctional changes of the astrocyte in rat hippocampus under different corticosteroid conditions. *Medical molecular morphology* 45:206–213. doi:[10.1007/s00795-011-0561-4](https://doi.org/10.1007/s00795-011-0561-4)
 61. Ye Y, Wang G, Wang H, Wang X (2011) Brain-derived neurotrophic factor (BDNF) infusion restored astrocytic plasticity in the hippocampus of a rat model of depression. *Neurosci Lett* 503:15–19. doi:[10.1016/j.neulet.2011.07.055](https://doi.org/10.1016/j.neulet.2011.07.055)
 62. You Y, Gupta VK, Graham SL, Klistorner A (2012) Anterograde degeneration along the visual pathway after optic nerve injury. *PLoS One* 7:e52061. doi:[10.1371/journal.pone.0052061](https://doi.org/10.1371/journal.pone.0052061)